J Mater Sci (2011) 46:4221–4227
DOI 10.1007/s10853-010-5236-3

IIB 2010

Deformation structure in ductile B2-type Zr–Co–Ni alloys with martensitic transformation

Mitsuhiro Matsuda · Takahiro Nishimoto · Kyohei Matsunaga · Yasuhiro Morizono · Sadahiro Tsurekawa · Minoru Nishida

Received: 30 August 2010 / Accepted: 30 December 2010 / Published online: 11 January 2011

Abstract Microstructural evolution during tensile deformation in ternary Zr–Co–Ni alloys were investigated using transmission electron microscopy to clarify the mechanism of the enhancement of ductility observed in these alloys. In $Zr_{50}Co_{39}Ni_{11}$ alloy deformed at room temperature, lenticular martensite is observed in the B2 parent phase immediately after yielding, in addition to dislocations with the $<100>_{B2}$-type Burgers vector. The orientation relationship between the B2 parent phase and B33 martensite is determined to be $[001]_{B2}//[100]_{B33}$, $(010)_{B2}//(021)_{B33}$, and $(110)_{B2}//(010)_{B33}$. A midrib-like contrast is observed at the center of the lenticular martensite variant, and it is found to be a $(021)_{B33}$ twin. A trace analysis indicates that this contrast is nearly parallel to the $\{100\}_{B2}$, which may correspond to the habit plane of the martensite. The martensite variants grow into the B2 parent phase along the $\{100\}_{B2}$ with increasing tensile loading, and then grid-shaped martensite variants are formed at the failure of the specimen. The martensite would be dominantly formed and grow in the regions where the stress concentration occurs during tensile deformation. It is likely that the plastic deformation mainly proceeds in the untransformed B2 parent phase because this martensite is harder than the B2 parent phase. Consequently, the authors conclude that the remarkable enhancement of ductility can be attributed to a transformation-induced plasticity associated with deformation-induced martensite.

M. Matsuda (✉) · T. Nishimoto · K. Matsunaga · Y. Morizono · S. Tsurekawa
Department of Materials Science and Engineering, Kumamoto University, 2-39-1 Kurokami, Kumamoto 860-8555, Japan
e-mail: matsuda@alpha.msre.kumamoto-u.ac.jp

M. Nishida
Department of Applied Science for Electronics and Materials, Kyushu University, Kasuga 816-8580, Japan

Introduction

Intermetallic compounds with both high hardness and high-temperature strength are essential materials for the development of scientific technology. However, most of these compounds exhibit very poor ductility at room temperature. Even a B2-type intermetallic compound generally has low ductility at room temperature in spite of its relatively simple crystal structure because slip systems are limited according to the ordering in alloys. Thus, methods to improve ductility have been explored, such as the addition of alloying elements and the control of microstructures [1, 2]. Among B2-type intermetallic compounds, near-equiatomic Ti-Ni alloys exhibit superior shape memory and superelastic properties. Another notable property of these alloys is anomalous ductility over a wide temperature range. This is attributable to an increase in the effective number of the slip system caused by a stress- and/or strain-induced martensitic transformation [3]. It was therefore expected that the tensile ductility of intermetallic compounds at room temperature will be further enhanced by martensitic transformation.

Recently, Takasugi and co-workers [4] have found that a polycrystalline B2-type equiatomic ZrCo compound has a high tensile elongation of 7% at room temperature. On the other hand, it has been found that an equiatomic ZrNi compound with a B33 structure is relatively brittle, and that the martensitic transformation from B2 to B33 structures takes place via the substitution of 14–50 at% Ni for Co [5, 6]. The authors have found a high ductility of a ZrCo alloy caused by martensitic transformation, and that the tensile

strength and elongation are significantly increased by the substitution of Ni for Co in ternary Zr–Co–Ni alloys [7]. In particular, the total elongation of the $Zr_{50}Co_{39}Ni_{11}$ alloy is considerably high, being approximately 23%. In this study, it was carried out transmission electron microscopy (TEM) observations of microstructural evolution during tensile deformation of ternary Zr–Co–Ni alloys with the aim of clarifying the mechanism of enhancement of ductility in these alloys.

Experimental procedures

$Zr_{50}Co_{50}$, $Zr_{50}Co_{39}Ni_{11}$ and $Zr_{50}Co_{36}Ni_{14}$ alloys were prepared from 99.9% Zr, 99.9% Co, and 99.9% Ni (mass%) by arc melting in an argon atmosphere. The ingots were cold-rolled into a strip of 0.3 mm in thickness. Tensile specimens with gauge sizes of $30 \times 5 \times 0.3$ mm^3 were spark-cut from the strip. The samples were solution-treated in an argon atmosphere at 1173 K for 3.6 ks and then quenched in iced water. The tensile tests were conducted using an Instron-type machine at room temperature. The initial strain rate of the tensile test was 4.2×10^{-4}/s. For the TEM studies, disks with 3 mm in diameter were spark-cut from the solution-treated specimens and from the gauge portion of the tensile specimens deformed to various residual strains. They were then electropolished by a twin-jet method in an electrolyte solution of 25% HNO_3 and 75% methanol by volume at around 238 K. Conventional and high-resolution TEM observations were carried out on a JEM-2000FX and FEI-Tecnai20F microscopes, respectively, with an accelerating voltage of 200 kV. For analysis, the following lattice parameters were used: $a_{B2} = 0.320$, $a_{B33} = 0.325$, $b_{B33} = 0.971$, and $c_{B33} = 0.419$ nm [5].

Results and discussion

Figure 1 shows the typical tensile stress–strain curves at room temperature for ternary Zr–Co–Ni alloys substituting Ni for Co. A $Zr_{50}Co_{50}$ alloy has a 0.2% proof stress of 240 MPa and a total elongation of approximately 6%. These values are almost the same as those reported by Takasugi and co-workers [4]. A $Zr_{50}Co_{39}Ni_{11}$ alloy has a considerably high total elongation of 23%. On the other hand, a $Zr_{50}Co_{36}Ni_{14}$ alloy has a lower elongation than the $Zr_{50}Co_{50}$ alloy. In order to clarify the mechanism of the enhancement of ductility resulting from substituting of Ni for Co, the tensile tests for the $Zr_{50}Co_{39}Ni_{11}$ alloy specimens were interrupted, as shown by the dotted lines A and B in Fig. 1. Thereafter, TEM observations were carried out with the specimens A and B, in addition to the tensile-fractured specimens of $Zr_{50}Co_{39}Ni_{11}$ and $Zr_{50}Co_{36}Ni_{14}$

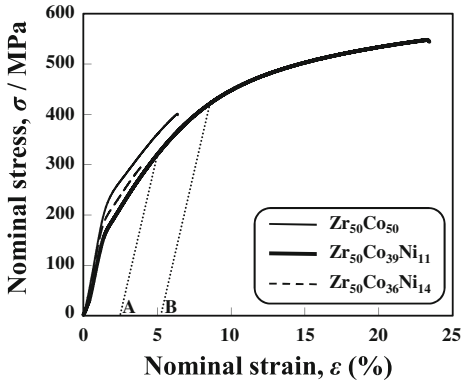

Fig. 1 Typical nominal stress–strain curves at room temperature for ternary Zr–Co–Ni alloys substituting Ni for Co

alloys. Figure 2 shows the TEM micrographs of Zr–Co and Zr–Co–Ni alloys before deformation. The $Zr_{50}Co_{50}$ and the $Zr_{50}Co_{39}Ni_{11}$ alloys consist of a single phase with B2 structure, the average grain sizes being approximately 5 μm. The electron diffraction pattern taken from the area marked F in Fig. 2e reveals that B2 and B33 structures coexist in the $Zr_{50}Co_{36}Ni_{14}$ alloy. The orientation relationship between the B2 parent phase and B33 martensite is determined to be $[001]_{B2}//[100]_{B33}$, $(010)_{B2}//(021)_{B33}$, and $(110)_{B2}//(010)_{B33}$. This thermally-induced martensite consists of plate-shaped variants. Figure 3 displays the deformed microstructure of the $Zr_{50}Co_{39}Ni_{11}$ alloy specimen with a residual strain of approximately 2.5%, as indicated by the dotted line A in Fig. 1. Fine lenticular martensite variants were formed along the $\{100\}_{B2}$ of B2 parent grain. The orientation relationship between the parent grain and the martensite variants is determined to be $[001]_{B2}//[100]_{B33}$, $(010)_{B2}//(021)_{B33}$, and $(110)_{B2}//(010)_{B33}$. This relationship is the same as that between the B2 parent grain and thermally-induced B33 martensite, as shown in Fig. 2f. The deformation microstructure at a residual strain of approximately 5.0% (the dotted line B in Fig. 1) is shown in Fig. 4. The martensite variants grow into the parent grain along the $\{100\}_{B2}$ planes. It should be noted that a midrib-like contrast is observed at the center of the lenticular martensite variant. This contrast was found to come from a $(021)_{B33}$ twin, and a trace analysis revealed this contrast being nearly parallel to the $\{100\}_{B2}$ planes. Accordingly, the $\{100\}_{B2}$ planes would be the habit plane of this martensite. The twinning elements of the lenticular martensite are $K_1 = (021)_{B33}$, $K_2 = (0\bar{2}1)_{B33}$, $\eta_1 = [0\bar{1}2]_{B33}$, and $\eta_2 = [012]_{B33}$, as calculated according to the Bilby-Crocker theory [8]. The twinning shear is approximately 0.3. Figure 5 shows a two-dimensional lattice image of the tip of the lenticular martensite. The interface between the B2 parent grain and B33 martensite possesses a coherent structure, because the difference between the lattice spacings of $(110)_{B2}$ and $(010)_{B33}$ is small.

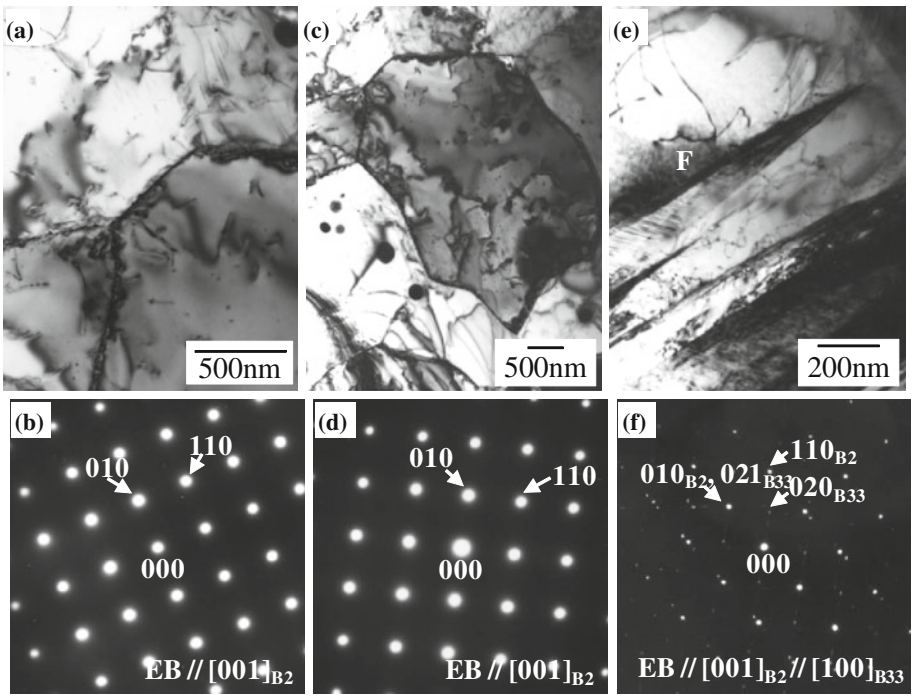

Fig. 2 Bright field images and corresponding electron diffraction patterns of **a**, **b** $Zr_{50}Co_{50}$ and **c**, **d** $Zr_{50}Co_{39}Ni_{11}$ alloys, showing a single phase with B2 structure, and **e**, **f** $Zr_{50}Co_{36}Ni_{14}$ alloy, which suggests the coexistence of B2 parent phase and B33 martensite

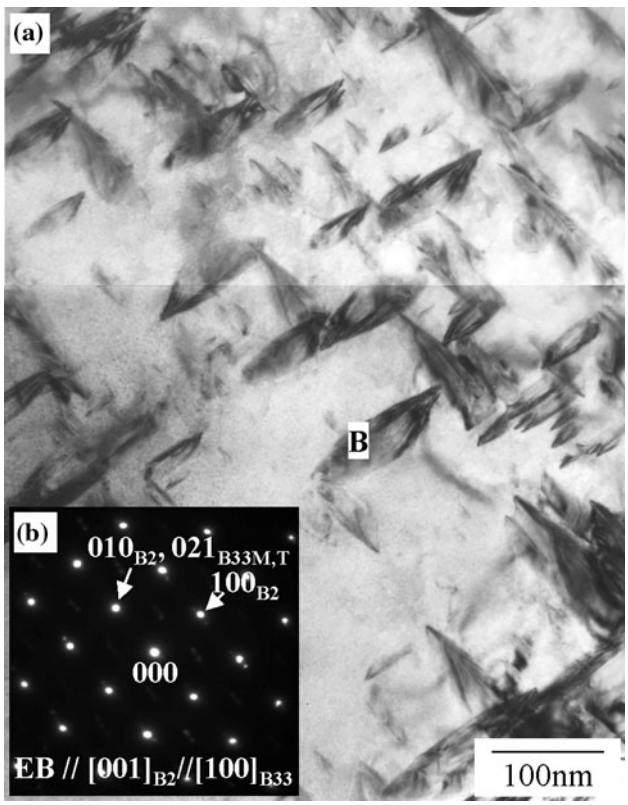

Fig. 3 **a** Bright field image of $Zr_{50}Co_{39}Ni_{11}$ alloy with a residual strain of approximately 2.5%. **b** Electron diffraction pattern taken from the area marked as B in (**a**)

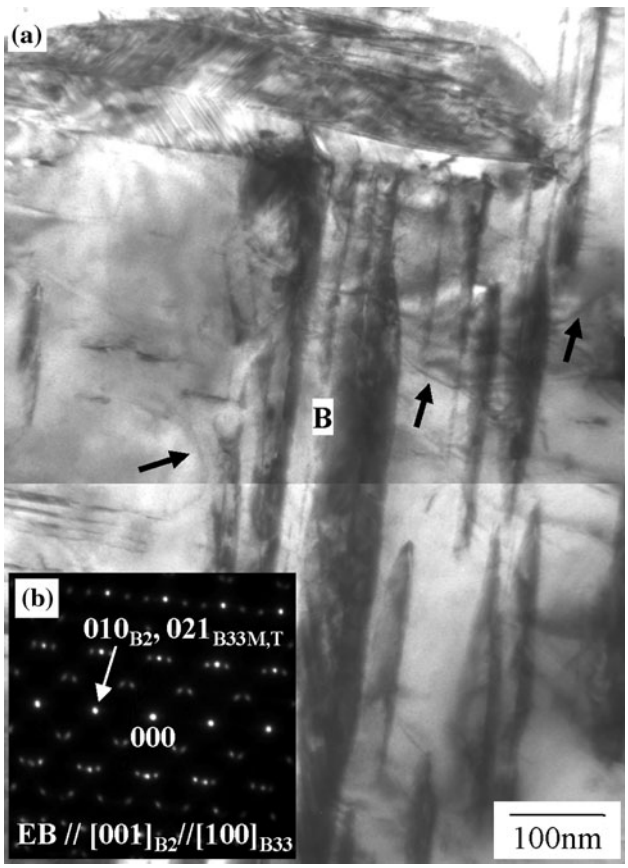

Fig. 4 **a** Bright field image of $Zr_{50}Co_{39}Ni_{11}$ alloy with a residual strain of approximately 5.0%. **b** Electron diffraction pattern taken from the area marked as B in (**a**)

Therefore, the lenticular martensite variants can grow by the migration of the coherent interface under the tensile loading. This feature is similar to the characteristics of thermoelastic martensite.

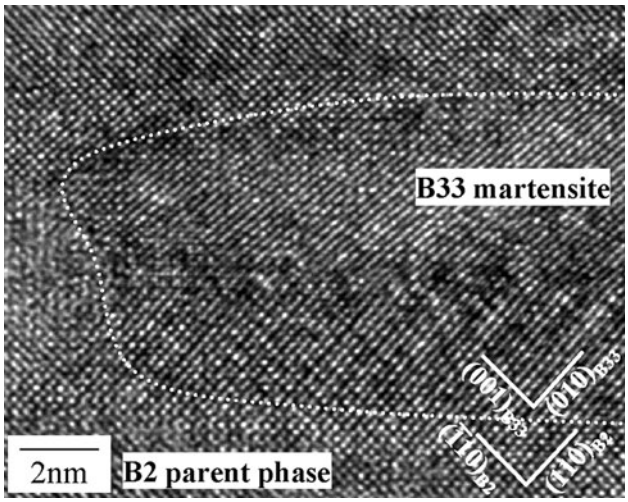

Fig. 5 Two-dimensional lattice image of the tip of lenticular martensite

It was identified the slip system of the B2 parent phase from the trace analysis, because many dislocations in the B2 parent phase were observed in addition to the lenticular martensite, as indicated by the arrows in Fig. 4. Figure 6 presents the dark field images of the $Zr_{50}Co_{39}Ni_{11}$ alloy specimen with a residual strain of approximately 5.0%. Each image was taken under a two-beam diffraction condition using the $\boldsymbol{g}$ vector shown in the figure with the incident electron beam from the $[001]_{B2}$ direction. Dislocations are visible under the diffraction conditions of $\boldsymbol{g} = 110$ and $\bar{1}10$, while they are invisible under the conditions of $\boldsymbol{g} = 100$ and 010. On the basis of the $\boldsymbol{g}\cdot\mathbf{b}$criterion, the authors can identify the Burgers vector of the dislocations as $<100>_{B2}$. In addition, stereographic analysis for the determination of slip plane of these dislocations was carried out, as demonstrated in Fig. 7. The planes normal to the incident beam $\boldsymbol{B_A}$, $\boldsymbol{B_B}$, $\boldsymbol{B_C}$, and $\boldsymbol{B_D}$ are shown in the stereogram as great circles (A), (B), (C), and (D), respectively. The projected line directions of an interest dislocation on (A), (B), (C), and (D) are indicated by $\boldsymbol{d_A}$, $\boldsymbol{d_B}$, $\boldsymbol{d_C}$, and $\boldsymbol{d_D}$, respectively. Hence, the true line direction of this dislocation, $\boldsymbol{U_d}$, is given as the intersection of the great circles whose poles are perpendicular to $\boldsymbol{d_A}$, $\boldsymbol{d_B}$, $\boldsymbol{d_C}$, and $\boldsymbol{d_D}$ on (A), (B), (C), and (D) planes, respectively.

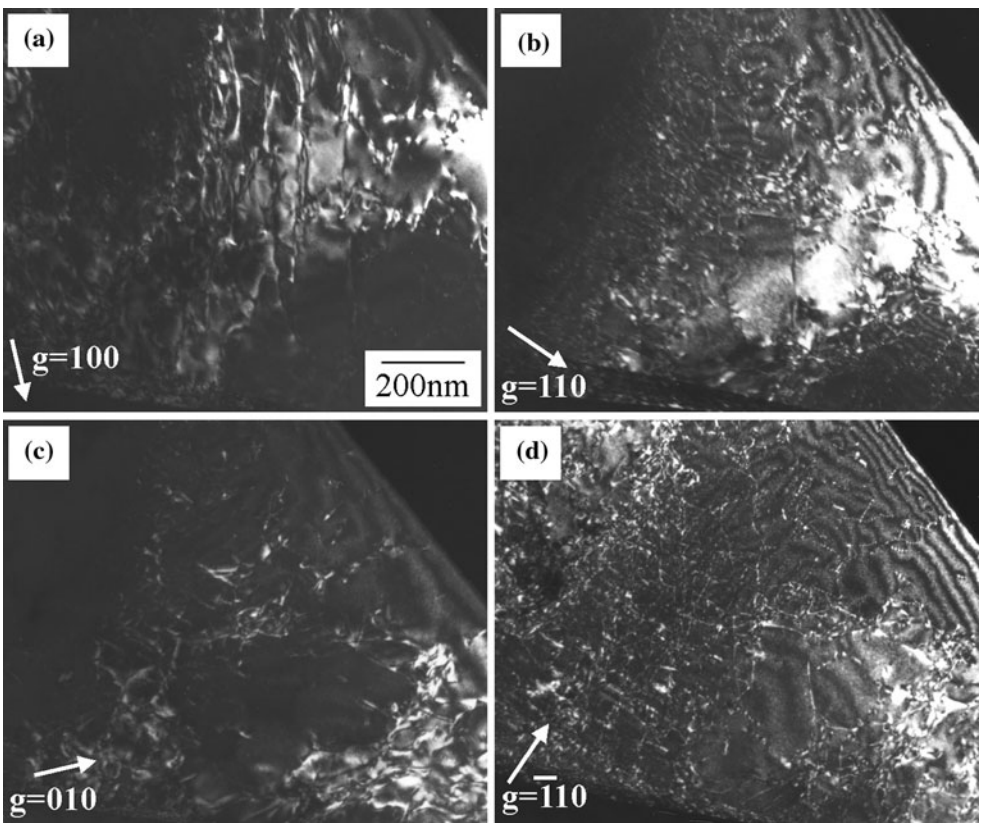

Fig. 6 Dark field images of $Zr_{50}Co_{39}Ni_{11}$ alloy with a residual strain of approximately 5.0%. **a** $\boldsymbol{g} = 100$. **b** $\boldsymbol{g} = 110$. **c** $\boldsymbol{g} = 010$, and **d** $\boldsymbol{g} = \bar{1}10$. The incident electron beam was nearly parallel to $[001]_{B2}$

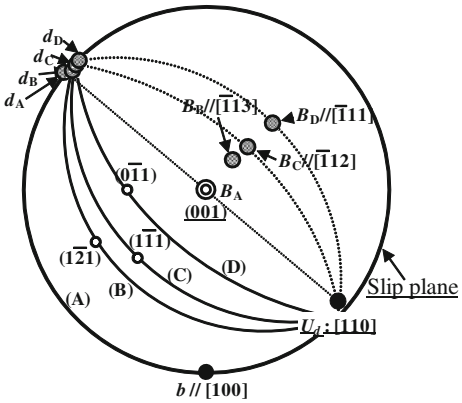

Fig. 7 Stereographic analysis for the determination of slip plane of dislocations in $Zr_{50}Co_{39}Ni_{11}$ alloy with a residual strain of approximately 5.0%

Consequently, the slip plane is given as a plane that contains both the Burgers vector, $\boldsymbol{b}$, and the true dislocation line direction, $\boldsymbol{U_d}$. The pole of this slip plane indicated by double circle is quite close to that of $(001)_{B2}$. It is therefore confirmed that the dislocation shown in Fig. 6 belongs to the $<100>(001)_{B2}$ slip system. Some dislocations with the $<100>\{011\}_{B2}$ slip system were observed in other regions as well. Since these are well-known slip systems among the B2-intermetallic compounds, including $Zr_{50}Co_{50}$ alloy, the origin of higher ductility in the $Zr_{50}Co_{39}Ni_{11}$ alloy cannot be explained by the observed slip system itself.

The microstructure observed near the fractured area is shown in Fig. 8. The martensite variants grow into the B2 parent phase along the $\{100\}_{B2}$ with increasing tensile loading, and then grid-shaped martensite variants are formed in the fractured specimen. It is noteworthy that the interface migration of martensite variants perpendicular to their growth direction is restricted. Therefore, the migration of the twin boundary between the grid-shaped martensite variants is limited, depending on the tensile direction. This suggests that the ductility of the martensite itself is low. The authors will discuss the origin of the enhancement of ductility on the basis of the deformation structure in $Zr_{50}Co_{36}Ni_{11}$ alloy in the following part of this article.

It was carried out TEM observations of the area near the fracture surface of the $Zr_{50}Co_{36}Ni_{14}$ alloy with the lower elongation. As shown in Fig. 2, this alloy was initially composed of the B2 parent phase and the thermally-induced B33 martensitic phase at room temperature. Two different morphologies of martensite variants are observed after deformation as shown in Fig. 9. It is well-known that twin boundary migration and the rearrangement of variants in thermoelastic martensite take place with loading [9]. Figure 9a reveals that the width of twins in martensite increases during tensile deformation, that is, variant

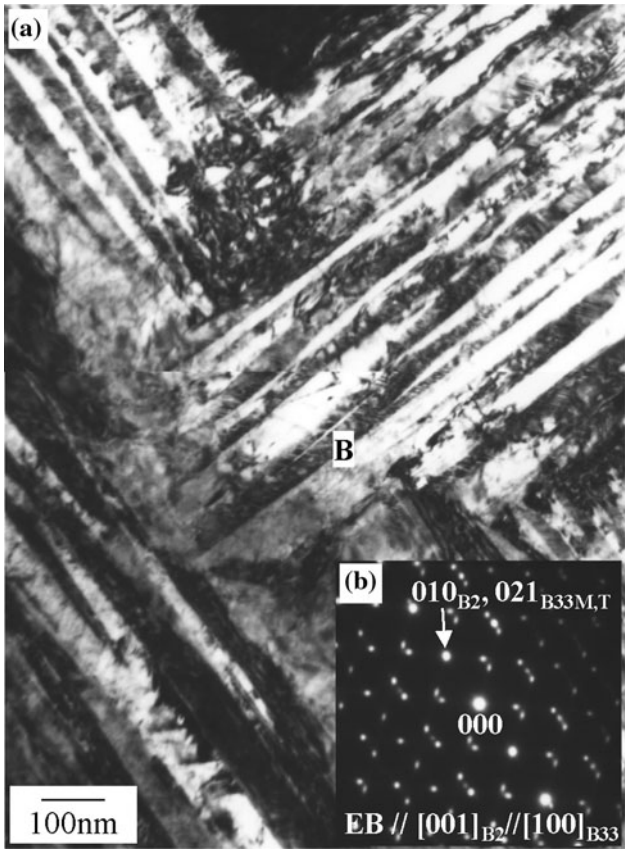

Fig. 8 **a** Bright field image near the fractured area of $Zr_{50}Co_{39}Ni_{11}$ alloy. **b** Electron diffraction pattern taken from the area marked as B in (**a**)

coalescence may have taken place via the growth of the most favorable variants with respect to the tensile axis. On the other hand, Fig. 9b shows that martensite platelets appear to be sheared by tensile deformation, as indicated by the arrows in Fig. 9b. This suggests that thermally induced martensite will behave as brittle nature when the configuration of plate-shaped variants is an unfavorable condition for occurring variant rearrangement. Therefore, it is considered that the thermally-induced B33 martensite would cause a decrease in ductility of the $Zr_{50}Co_{36}Ni_{14}$ alloy.

From these observations, the mechanism of the enhancement of ductility in ternary Zr–Co–Ni alloys will be discussed. The lenticular martensite is nucleated and grows along $\{100\}_{B2}$ during tensile deformation immediately after yielding. The growth direction of the martensite variants is the same as the Burgers vector of dislocations in the B2 parent phase. Thus, the formation of deformation-induced martensite cannot contribute to increasing the number of the independent slip systems in this alloy. Next, the authors will consider whether the lattice deformation strain associated with martensitic transformation can explain the enhancement of ductility. The principal lattice deformation strains arising from the lattice correspondence

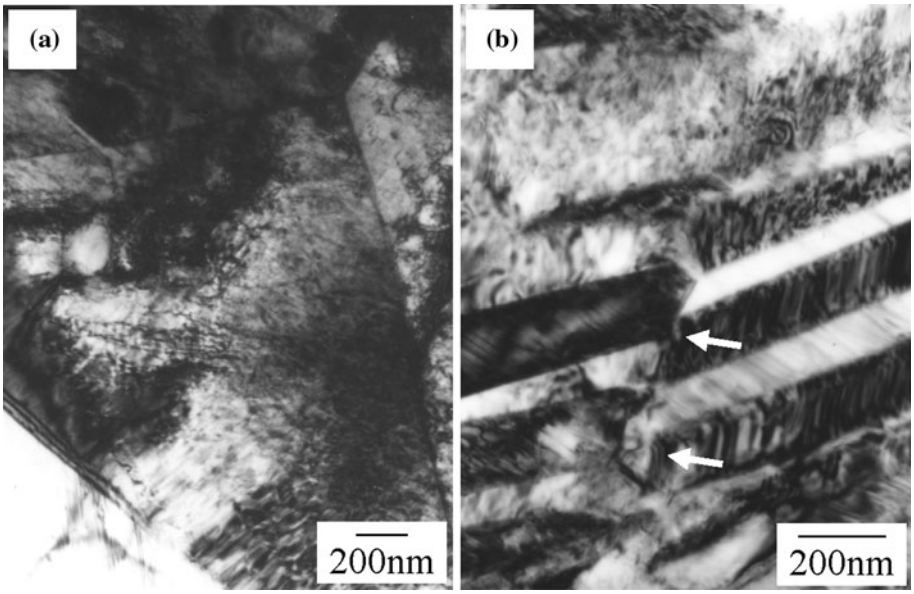

Fig. 9 Bright field images near the fractured area of $Zr_{50}Co_{36}Ni_{14}$ alloy, showing **a** martensite variant coalescence **b** martensite platelets sheared by tensile deformation

between the B2 parent phase and B33 martensite are as follows:

$$\eta_1 = (a_{B33} - a_{B2})/a_{B2} = 0.016$$

$$\eta_2 = (b_{B33} - 2\sqrt{2}a_{B2})/2\sqrt{2}a_{B2} = 0.073$$

$$\eta_3 = (c_{B33} - \sqrt{2}a_{B2})/\sqrt{2}a_{B2} = -0.074$$

The volume change due to the martensitic transformation is found to be small. Furthermore, the twinning shear of the lenticular martensite is nearly the same as that of general thermoelastic martensite [10]. Therefore, the origin of higher ductility also cannot be attributed to introducing deformation strains involved in martensitic transformation.

A possible scenario for the enhancement of ductility is as follows. The martensite would be formed and grow in the region where the stress concentration occurs during tensile deformation. Because the B33 martensite is harder than the B2 parent phase [7], the formation of this martensite is likely to prevent further local deformation occurring at the stress-concentrated area, and then achieves enhanced ductility. Consequently, it was concluded that the remarkable enhancement of ductility can be attributed to a transformation-induced plasticity associated with deformation-induced martensite [11].

Finally, the authors would like to offer some comments concerning the relationship between the martensitic structure and characteristics in these alloys. In the case of thermoelastic martensite, the martensitic phase is softer than the parent phase. On the other hand, in case of non-thermoelastic martensite, the martensitic phase is harder than the parent phase. From this point of view, the martensite in these alloys is classified as the category of non-thermoelastic martensite. However, the lenticular martensite variants can grow during tensile deformation. This is a characteristic of the thermoelastic martensite transformation. That is to say, the martensite in Zr–Co–Ni alloys may possess characteristics of both thermal and non-thermal martensitic transformation. Consequently, it is expected that Zr–Co–Ni alloys will show the shape memory and superelastic behavior arising from the thermoelastic martensite, in addition to the transformed strengthening and transformation-induced plasticity effect from the non-thermoelastic martensite.

Conclusions

Microstructural evolution during tensile deformation of ternary Zr–Co–Ni alloys were investigated by transmission electron microscopy in order to reveal the mechanism of the enhancement of ductility observed in these alloys. The obtained results are summarized as follows.

(1). In the $Zr_{50}Co_{39}Ni_{11}$ alloy deformed at room temperature, lenticular martensite was observed in the B2 parent phase immediately after yielding, in addition to dislocations with the $<100>_{B2}$-type Burgers vector. The martensite variants grew along the $\{100\}_{B2}$ planes in the parent grain. The orientation relationship between the B2 parent phase and the B33 martensite was determined to be $[001]_{B2}//[100]_{B33}$, $(010)_{B2}//(021)_{B33}$, and $(110)_{B2}//(010)_{B33}$.

(2). A midrib-like contrast was observed at the center of the lenticular martensite variant, and it was found to be the $(021)_{B33}$ twin. A trace analysis revealed that this contrast is nearly parallel to the $\{100\}_{B2}$, which may correspond to the habit plane of the martensite.

(3). The morphology of martensite variants changed into grid-shaped martensite variants during tensile deformation. The martensite interface perpendicular to the growth direction of martensite variants was hardly to migrate.

(4). The $Zr_{50}Co_{36}Ni_{14}$ alloy consisting of the B2 parent phase and the B33 thermally-induced martensite possessed a lower elongation than the $Zr_{50}Co_{50}$ alloy. This suggests that the B33 martensite itself in Zr–Co–Ni alloys would be intrinsically brittle.

(5). The B33 martensite was dominantly formed and grew in the region where a stress concentration occurred during tensile deformation. The deformation in the untransformed B2 parent phase probably contributed to overall elongation of the specimen, rather than the deformation of the martensite, because this martensite is harder than the B2 parent phase. Consequently, it was concluded that the pronounced enhancement of ductility can be attributed to the transformation-induced plasticity associated with the deformation-induced martensite.

Acknowledgements This study was supported by a "Grant-in-Aid for Scientific Research (B)" from the Japanese Society for the Promotion of Science (JSPS)" and a "Grant-in-Aid for Young Scientists (B)" from the Ministry of Education, Culture, Sports, Science and Technology (MEXT), Japan.

References

1. Ishida K, Kainuma R, Ueno N, Nishizawa T (1991) Metall Trans 22A:441
2. Tawancy HM, Aboelfotoh MO (2010) J Mater Sci 45:3413. doi: 10.1007/s10853-010-4366-y
3. Nishida M, Tanaka K, Ii S, Kohshima M, Miura S, Asai M (2003) J Phys IV 112:803
4. Yamaguchi T, Kaneno Y, Takasugi T (2005) Scr Mater 52:39
5. Carvalho EM, Harris IR (1985) J Less-Common Metals 106:143
6. Hossain D, Harris IR, Barraclough KG (1974) J Less-Common Metals 37:35
7. Matsuda M, Hayashi K, Nishida M (2009) Mater Trans 50:2335
8. Bilby BA, Crocker AG (1965) Proc of Roy Soc Ser A 288:240
9. Mohamed HA, Washburn J (1977) J Mater Sci 12:469. doi: 10.1007/BF00540269
10. Adachi K (1988) Bull Japan Inst Metals 1:21
11. Tamura I, Maki T (1971) In: Proceedings of the international conference on toward improved ductility and toughness, Kyoto, pp 183–193